Development of the Personalized Chinese Adult Mesh Phantom Library for Accurate Computed Tomography Dose Evaluation

Authors: Zhang, Zhijie, Xinliang Lu, Liu, Yuhang, Kang, Prof. Tianliang, Zhang, Prof. Yongxian, Liu, Prof. Dandan, Hu, Prof. Yanjun, QIU, Dr. RUI 邱睿, Dr. Lihua Zhu, wang, Prof. zhengchang, Prof. Yantao Niu, Prof. Yantao Niu

Date: 2025-10-29T00:00:00+00:00

Abstract

Computed tomography (CT) is an indispensable tool in clinical diagnosis. Nevertheless, it also involves non-negligible risks due to exposure to ionizing radiation. To accurately evaluate the radiation dose received by Chinese adults during CT examinations, we analyze the relationships between body size, organ mass, and anthropometric parameters in the Chinese adult population. Anatomical contours obtained from clinical images are used to develop the Chinese Adult Mesh Phantom (CAMP) library, each containing 121 organs and tissues. Compared with the ICRP (International Commission on Radiological Protection) Mesh-type Reference Computational Phantoms (MRCPs), the CAMP exhibits markedly reduced relative errors in organ masses. For the male phantom, the relative error of liver mass decreased from 67.38% to 2.44%, spleen mass from 47.35% to 3.89%, and pancreas mass from 44.69% to 8.08%. For the female phantom, the relative error of liver mass decreased from 40.31% to 9.53%, stomach mass from 50.01% to 10.35%, and breast mass from 70.77% to 12.51%. Compared with the Chinese national standard anatomical reference data, the organ masses in the normal body size polygon mesh model show discrepancies within approximately 10%. Furthermore, the organ masses and morphologies of the phantoms representing different body sizes remain anatomically realistic and clinically consistent. Ultimately, we establish a cohort of mesh phantoms that accurately represent Chinese adults. We present a comprehensive system for estimating organ doses in CT examinations and offer valuable insights for optimizing CT imaging protocols and assessing patient radiation exposure.

Full Text

Preamble

Title: Development of the Personalized Chinese Adult Mesh Phantom Library for Accurate Computed Tomography Dose Evaluation

Authors: Zhijie Zhang[1],[2], Dandan Liu[3], Yanjun Hu[1], Yantao Niu[1],, *Xinliang Lu*[3], *Yuhang Liu*[3], *Rui Qiu*[4], *Tianliang Kang*[3], *Yongxian Zhenchang Wang*[1],, Lihua Zhu[2],*

Affiliations: [1]Department of Radiology, Beijing Friendship Hospital, Capital Medical University, Beijing 100050, China
[2]School of Physics, Beihang University, Beijing 102206, China
[3]Department of Radiology, Beijing Tongren Hospital, Capital Medical University, Beijing 100730, China
[4]Department of Engineering Physics, Tsinghua University, Beijing 100084, China

*Corresponding authors: zhulh@buaa.edu.cn; ytniu163@163.com; cjr.wzhch@vip.163.com

Abstract: Computed tomography (CT) is an indispensable tool in clinical diagnosis, yet it involves non-negligible risks due to exposure to ionizing radiation. To accurately evaluate the radiation dose received by Chinese adults during CT examinations, we analyzed the relationships between body size, organ mass, and anthropometric parameters in the Chinese adult population. Anatomical contours obtained from clinical images were used to develop the Chinese Adult Mesh Phantom (CAMP) library, with each phantom containing 121 organs and tissues. Compared with the ICRP (International Commission on Radiological Protection) Mesh-type Reference Computational Phantoms (MRCPs), the CAMP exhibited markedly reduced relative errors in organ masses. For the male phantom, the relative error of liver mass decreased from 67.38% to 2.44%, spleen mass from 47.35% to 3.89%, and pancreas mass from 44.69% to 8.08%. For the female phantom, the relative error of liver mass decreased from 40.31% to 9.53%, stomach mass from 50.01% to 10.35%, and breast mass from 70.77% to 12.51%. Compared with Chinese national standard anatomical reference data, organ masses in the normal body size polygon mesh model show discrepancies within approximately 10%. Furthermore, the organ masses and morphologies of phantoms representing different body sizes remain anatomically realistic and clinically consistent. Ultimately, we established a cohort of mesh phantoms that accurately represent Chinese adults and present a comprehensive system for estimating organ doses in CT examinations, offering valuable insights for optimizing CT imaging protocols and assessing patient radiation exposure.

Keywords: Computed tomography, Monte Carlo simulation, Chinese adult mesh phantom, organ dose

1. Introduction

Currently, more than one billion radiological diagnostic and therapeutic procedures are performed annually in China, contributing substantially to patient healthcare while simultaneously posing potential risks associated with ionizing radiation exposure [**?**]. In 2016, approximately 782 million radiological diagnostic procedures were conducted in China, with X-ray examinations accounting for 52.4%, computed tomography (CT) scans for 37.1%, interventional radiology for 0.7%, and nuclear medicine for 1.1% [**?**]. According to the 2020/2021 report of the United Nations Scientific Committee on the Effects of Atomic Radiation (UNSCEAR), CT examinations contributed up to 61.6% of the collective effective dose from all radiological imaging procedures [**?**]. A survey involving 3.2 million patients across 26 countries reveals that nearly 900,000 patients worldwide receive cumulative CT radiation doses exceeding 100 mSv each year [**?**]. Furthermore, CT-related cancers could eventually account for up to 5% of all newly diagnosed cancer cases annually at current CT utilization rates and dose levels [**?**]. Related studies have found a positive correlation between cumulative CT radiation exposure and the incidence of hematologic malignancies [**?**]. Overall, these findings underscore the critical importance of accurately quantifying radiation doses associated with CT examinations.

In clinical CT examinations, the tube current varies dynamically according to the patient' s body size, and the volume computed tomography dose index (CTDI(*{vol})) reported by the scanner, which is calculated using an average tube current, cannot accurately represent the absorbed dose to specific organs. Schlattl et al. demonstrated that when organ dose coefficients derived from fixed tube current conditions are combined with scanner-reported CTDI(*{vol}) to estimate organ doses, the resulting dose errors can exceed 50% [**?**]. Monte Carlo (MC) simulation is widely recognized as the most accurate method for radiation dose assessment and plays a pivotal role in fields such as nuclear engineering, radiation therapy, and diagnostic radiology. In CT dose evaluation, MC simulation estimates patient radiation exposure by modeling the energy deposition of a large number of particles interacting with human tissues. Samei et al. reported organ dose reference values for chest and abdominal CT examinations under different scanning conditions using MC simulations [**?**].

However, due to substantial differences in body size and composition between Western and Chinese adults, organ dose reference values derived from Western body models cannot be directly applied to Chinese patients. Therefore, it is essential to develop CT radiation dose assessment tools tailored to Chinese adult body characteristics and to establish corresponding reference dose data for clinical applications.

As a widely adopted technique for radiation dose estimation in diagnostic radiology, the accuracy of MC simulation largely depends on the computational phantom employed. The development of computational phantoms has evolved through three major stages, including mathematical, voxel-based, and mesh-

based phantoms [?]. Mathematical phantoms represent organs and tissues using simple geometric shapes such as ellipsoids, cones, and elliptical cylinders. In the early era of limited computing power, these simplified anatomical models were frequently employed in MC simulations due to their simplicity, computational efficiency, and ease of adjustment, and they played an essential role in the establishment of international radiation protection standards [?]. In 1969, Snyder et al. developed the MIRD-5 (Medical Internal Radiation Dosimetry) phantom to represent average human anatomical characteristics [?]. However, because of extensive anatomical simplifications, mathematical phantoms were unable to accurately capture the complexity of human anatomy.

Voxel phantoms emerged with the advancement of CT imaging technology. These phantoms are constructed by stacking a large number of voxels, each assigned a unique identifier corresponding to a specific anatomical structure. Unlike mathematical phantoms, voxel phantoms are derived from actual anatomical images, thereby providing a higher degree of anatomical realism and consequently have been widely used in radiation dose assessment research. In recent decades, extensive research efforts have been devoted to the development of voxel phantoms. Xu et al. developed a series of voxel phantoms, including VIP-Man and a pregnant female model [?]. Bolch et al. constructed the UF series of pediatric voxel phantoms [?]. Similarly, Zankl et al. created the GSF series of voxel phantoms based on multiple individuals [?]. To date, hundreds of voxel phantoms have been developed worldwide, covering a wide range of sex, body size, age groups, and stages of pregnancy [?]. Nevertheless, the construction of voxel phantoms is constrained by the spatial resolution of CT imaging systems, resulting in stair-step artifacts on phantom surfaces and relatively limited modeling accuracy for very small or anatomically complex structures [?].

Mesh-type computational phantoms are constructed using non-uniform rational B-splines (NURBS) and polygon meshes (PM) to represent organs. The quality and accuracy of these phantoms depend on the density and distribution of the mesh, enabling smoother surfaces and more detailed representation of human anatomy. In 2001, Segars developed the first mesh-type phantom, and this modeling approach offers distinct advantages in describing anatomical deformations [?]. In 2005, Xu et al. introduced a series of mesh phantoms, including RPI-AM, RPI-AF, and the RPI-pregnant female model [?]. Kim et al. developed the Mesh-type Reference Computational Phantoms (MRCP), which were published in ICRP Publication 145 in 2020 [?]. In 2024, ICRP Publication 156 introduced the Paediatric Mesh-type Reference Computational Phantoms [?, ?]. In addition, Ma et al. developed Chinese pediatric reference mesh phantoms for evaluating radiation doses in pediatric CT examinations [?]. Luo et al. constructed a series of Chinese adult standing phantoms to account for variations in body size [?]. Xie et al. developed a library of individualized pregnant female and fetal phantoms, including 46 phantoms spanning gestational weeks 0–9, as well as 30 Chinese reference mesh phantoms of different ages and 29 individualized pediatric computational phantoms \cite{24-26}.

Although numerous studies have constructed computational phantoms for Chinese adults, most existing individualized voxel models are generated by scaling standard reference models without accounting for variations in internal organs, and the external body contours often lack corresponding anthropometric reference data. In addition, these phantoms have not been extensively applied in clinical radiation protection and therefore have provided limited practical benefit in clinical settings. Consequently, developing highly individualized computational models for Chinese adults is essential for improving the accuracy of radiation dose estimation. To address these limitations, we developed the Chinese Adult Mesh-type Phantoms (CAMP) series, which incorporates body shape characteristics and organ mass properties representative of the Chinese adult population. Furthermore, we established conversion coefficients between clinical dose indices and organ doses using a self-developed CT radiation dose simulation program, providing a practical reference for rapid and accurate estimation of organ doses in CT examinations.

2.1 Analysis of Individualized Characteristics in Chinese Adults

The attenuation of X-rays varies among patients with different body sizes, and organ masses also differ among adults of varying physiques. Our goal is to establish a Chinese Adult Mesh-type Phantom library comprising eight representative models that reflect differences in body size (underweight, normal weight, overweight, and obese) and sex (male and female).

2.1.1 The Relationship Between Organ Mass and Body Weight

Strong positive correlations have been observed between body weight and the masses of the heart, liver, and spleen [**?**]. Similar but weaker associations exist for the lungs and kidneys, whereas brain mass is independent of body weight but strongly negatively correlated with age [**?**]. At the same body weight, male organs tend to be heavier than those of females, except for the liver. Wang et al. reported regression equations of organ weight against body weight based on autopsy records collected from anatomy, pathology, and forensic departments of major medical schools across China [**?**]. These analyses confirm a linear correlation between organ mass and body weight, with specific regression parameters presented in Table 1 .

Table 1 Regression equation of organ weight (Y) versus body weight (X): $Y=\alpha+\beta X$. Organs: Brain, Heart, Kidneys, Liver, Pancreas, Spleen. Female.

2.1.2 The Relationships Between Human Dimensions and Height and Weight

A clear correlation exists between human body dimensions and both height and weight [**?**]. To quantify the relationship between adult body dimensions, height, and weight in the Chinese population, we utilized data from GB/T

10000-2023 *Human dimensions of Chinese adults*, which presents fundamental statistics of human dimensions (upper arm circumference, chest circumference, waist circumference, hip circumference, and thigh circumference) across different percentiles and age groups (18–25, 26–35, 36–60, and 61–70 years) [**?**]. Linear regression was performed to obtain the relation between human dimensions and height and weight, and the regression coefficients are listed in Table 2 .

Table 2 Regression equation of body dimension (Y, cm) versus height (H, cm) and weight (W, kg): Human Dimension: Upper arm circumference, Chest circumference, Waist circumference, Hip circumference, Thigh circumference. Female.

2.2.1 Construction of a Mesh-type Phantom for Chinese Adults with Normal Body Size

In this study, polygonal mesh is primarily employed to construct the mesh-type phantoms, and the overall generation process is illustrated in Fig. 1

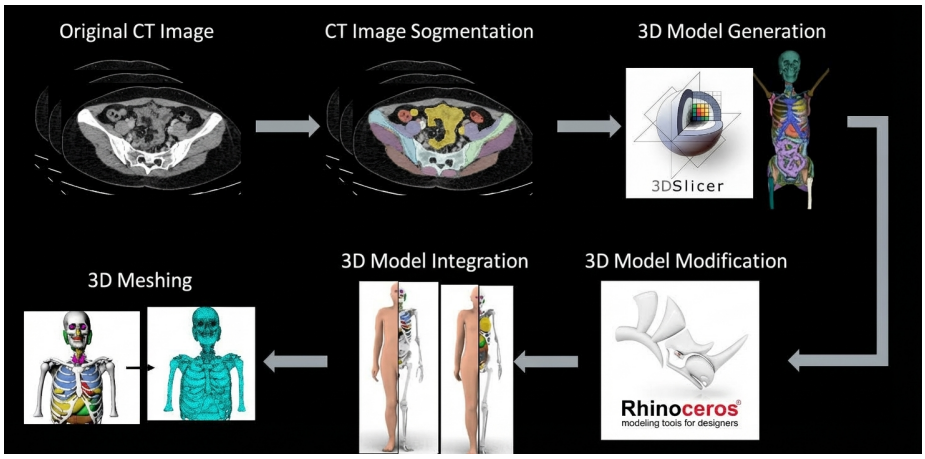

Figure 1: Figure 1

. First, all organs and tissues are delineated on CT images. To accelerate this process, the TotalSegmentator algorithm is applied to achieve automatic segmentation of 117 individual organs and tissues [**?**, **?**]. The CT images and corresponding masks are then imported into the 3D Slicer software for visualization, where regions with poor segmentation accuracy are manually corrected and re-delineated. Subsequently, the delineated organ contours are exported as PM models while preserving the relative anatomical positions of the original CT images, which are essential for subsequent model integration.

The individual organ models are further refined in Rhinoceros software to improve surface quality and anatomical consistency. The sizes of organ models are adjusted using offset commands and deformation controllers to ensure their

masses match reference values. Considering that small head organs and skeletal structures show minimal variation across adults of different body sizes, we focus primarily on constructing thoracic and abdominal organ models. The head organs and skeletal structures are transplanted from the MRCP model and further refined according to the specific requirements of this study. After optimization, the models are assembled, and their anatomical positions are carefully refined based on established anatomical knowledge. Inevitably, overlapping geometries arose during the assembly process, and resolving these conflicts while preserving anatomical plausibility presented substantial challenges. To address this issue, a priority ranking is assigned to each organ. Dense organs and those with clinically important or morphologically distinct features are given higher priority and preserved with minimal modification.

Organ integration is first performed using deformation controllers to smooth organ surfaces and maintain anatomical consistency. When deformation alone is insufficient to eliminate overlap, Boolean subtraction operations are applied to separate intersecting regions. Since Boolean subtraction can create visible cross-sections and reduce anatomical realism, it is applied only to minor overlaps to limit artifacts. When both deformation and subtraction prove insufficient, manual adjustment of mesh control points is used to separate overlapping regions while maintaining organ masses consistent with reference values. These three strategies are applied iteratively until all inter-organ overlaps are eliminated. For hollow organs such as the stomach, gallbladder, and bladder, the initial models exported from 3D Slicer represented solid structures in which organ walls and contents are merged. To differentiate these components, the solid model is defined as the organ wall, and an inner offset along the average normal direction is applied to generate the luminal volume.

After assembling the complete human body model, the polygonal mesh is converted into a tetrahedral mesh using the POLY2TET program [**?**].

Fig. 1 Overall Workflow for Constructing Mesh-type Phantoms

2.2.2 Construction of Mesh-type Phantoms for Chinese Adults with Other Body Sizes

Rather than merely scaling a standard reference phantom, we construct individualized mesh-type phantoms to better capture anatomical variability. Each individualized phantom is constructed independently following the method described in Section 2.2.1, with organ masses adjusted to match reference values calculated based on the equations in Table 1. Although this approach increases the modeling workload, it yields phantoms that more accurately represent the physiological characteristics of Chinese adults across different body sizes. Compared with the standard phantom, the most significant differences in individualized phantoms are observed in the skin and adipose layers. Therefore, we primarily focus on deforming the skin and soft tissue to align the phantom morphology with individualized anthropometric dimensions.

The skin of the normal body size phantom is used as the initial model, around which a deformation controller is established. Since the skin occupies a large volume, a relatively high number of control points is required to achieve fine adjustments. In this study, the number of control points along the X, Y, and Z axes is set to 24, 24, and 32, respectively. The control points corresponding to regions such as the upper arm, chest, waist, hip, and thigh circumferences are individually adjusted to deform the skin surface. According to previous studies, male adipose tissue tends to accumulate centripetally, concentrating in the trunk, particularly in the waist, abdomen, and around the navel, whereas female adipose tissue is more distributed in the chest, lower abdomen, and hips [**?**]. This distribution pattern is taken into account when adjusting the skin, and body dimensions are iteratively calculated and corrected until the deformed skin matches the reference measurements. Soft tissue is generated by inwardly offsetting the skin surface, followed by further refinement to ensure the overall phantom mass is consistent with reference values.

2.3 Development of a CT Radiation Dose Simulation System

A computational model of the PHILIPS IQon Spectral CT scanner is developed to construct a CT radiation dose simulation system. The X-ray spectrum is defined using the UserSpectrum command in GATE, with spectra generated by Spektr 3.0 software \cite{35–38}. Previously published CT scanner bowtie filter parameters are used as references \cite{39–42}. Additionally, following the method proposed by Yang et al., the bowtie filter of the PHILIPS IQon Spectral CT is independently measured [**?**, **?**]. The resulting filter profile is summarized in Table 3 .

Table 3 Aluminum equivalent thickness of the bowtie filter at different distances from the center point: d (cm), thickness (cm); d (cm), thickness (cm).

To validate the accuracy of the CT radiation dose simulation system developed in this study, organ doses are first measured in a physical dose phantom under actual CT scanning conditions. A corresponding voxel phantom is then constructed computationally, and organ doses are calculated using Monte Carlo simulations for comparison. The ART-200A-5 male dose phantom (manufactured by RSD, USA) and the PHILIPS IQon Spectral CT scanner are employed to assess the performance of the simulation system. The simulated organ doses deviated by less than 10% from the measured values. Considering additional uncertainties arising from scout scans, material conversion, and typical error levels reported in related studies, the proposed method can be regarded as capable of accurately estimating organ doses during clinical CT examinations [**?**].

2.4 Evaluation of Patient Organ Doses in Routine Chest and Abdominal CT Examinations

In this study, dose data from chest and abdominal CT scans of 21 subjects (7 males and 14 females) are collected to investigate the relationships among

CTDI(_{vol}), DLP (dose-length product), SSDE (size-specific dose estimates), and organ doses. During automatic tube current modulation (ATCM), the tube current varies along different axial positions of the patient. Organ doses for the entire scan are calculated by summing the products of the organ dose per single axial slice and the corresponding tube current at each position. To determine tube currents at different axial locations, a Python program is implemented using the Pydicom library to extract tube current distributions from the original DICOM files. Conversion factors between organ doses and CT radiation metrics are derived by fitting the measured organ doses to the corresponding CT dose indices. These factors enable rapid estimation of organ doses for selected organs in routine thoracoabdominal CT examinations.

3.1 Construction Results of the Personalized Mesh Phantom Library for Chinese Adults

CT images of 52 Chinese adults aged 20–50 years are collected, covering individuals with different body sizes and primarily involving the thoracic, abdominal, and pelvic regions. According to the Chinese BMI classification standard, underweight is defined as BMI < 18.5, normal weight as $18.5 \leq$ BMI < 24, overweight as $24 \leq$ BMI < 28, and obesity as BMI ≥ 28. Using the aforementioned methodology, a total of eight individualized mesh-type phantoms representing Chinese adult males and females of different body sizes are constructed. The male models include underweight (H = 176 cm, W = 53 kg, BMI = 16.73), normal (H = 176 cm, W = 68 kg, BMI = 21.47), overweight (H = 176 cm, W = 82 kg, BMI = 26.17), and obese (H = 176 cm, W = 98 kg, BMI = 32.00). The female models include underweight (H = 163 cm, W = 44 kg, BMI = 16.97), normal (H = 163 cm, W = 58 kg, BMI = 21.83), overweight (H = 163 cm, W = 69 kg, BMI = 25.34), and obese (H = 163 cm, W = 84.5 kg, BMI = 29.59). Fig. 2

shows render images of the phantom library, while Fig. 3 [FIGURE:3] presents renderings after removal of skin, soft tissue, and muscle.

As shown in Tables 4 and 5, the organ masses of the MRCP model exhibit substantial deviations from Chinese national reference values, with maximum relative errors of 67.38% for male organs and 70.77% for female organs, further demonstrating the necessity of developing Chinese-specific computational phantoms. In contrast, organ mass deviations of the models constructed in this study are controlled within 10% of the reference values. The CAMP corrected the discrepancies between MRCP organ masses and Chinese reference values, enabling more accurate estimation of organ and effective doses for Chinese adult patients. Compared with the international reference phantom MRCP, the CAMP models show significantly reduced relative errors in organ masses. For the male phantom, the relative error of liver mass decreased from 67.38% to 2.44%, spleen mass from 47.35% to 3.89%, and pancreas mass from 44.69% to 8.08%. For the female phantom, the relative error of liver mass decreased from 40.31% to 9.53%, stomach mass from 50.01% to 10.35%, and breast mass from 70.77% to 12.51%. When compared with Chinese national anatomical reference data,

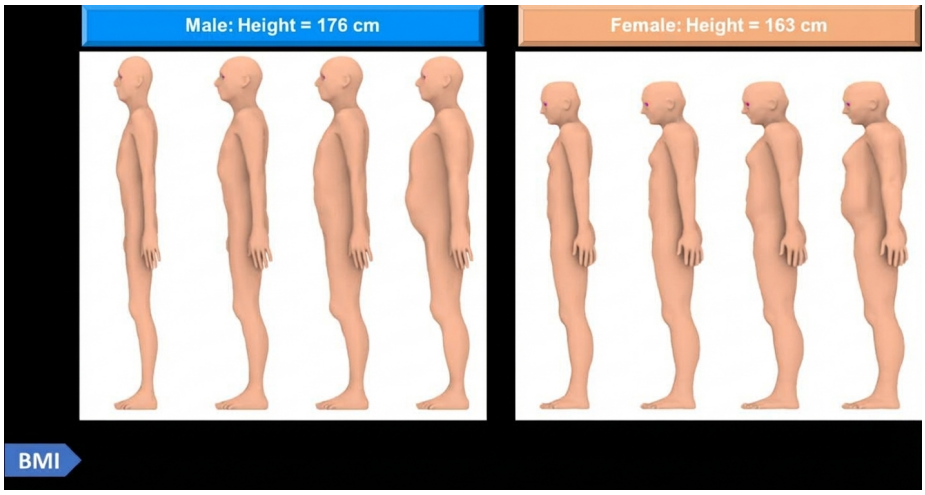

Figure 2: Figure 2

the differences in organ masses of the normal body-type CAMP were within approximately 10%.

Table 6 compares the organ weights of individualized Chinese phantoms with corresponding reference values. Among these, brain weight showed no significant variation across different body sizes, while the weights of the heart, kidneys, liver, lungs, pancreas, and spleen increased with body weight. Table 7 presents the anthropometric measurements of the individualized Chinese phantom models.

The CAMP series developed in this study includes eight models representing four body sizes for both males and females, with body dimensions and organ masses that more accurately reflect the characteristics of Chinese adults. Compared with the MRCP phantoms recommended in ICRP Publication 145, the CAMP phantoms exhibit smaller organ mass errors and are therefore more suitable for evaluating and optimizing CT radiation doses in Chinese adults. However, this study has certain limitations. The current models primarily focus on thoracic and abdominal organs; although variations in skeletal structures and small organs are relatively minor, their precise modeling requires further refinement in future work. In addition, the number of phantoms constructed remains limited, and individuals of different heights are not yet represented, which restricts the general applicability of the model library. The primary goal of this research is to establish a highly accurate and individualized mesh-type phantom population for the Chinese population and to integrate it closely with clinical applications to optimize patient radiation exposure in CT examinations. Future studies will focus on developing phantoms representing various heights and age groups, particularly constructing a Chinese pediatric mesh-type phantom series and advancing dose optimization strategies.

Fig. 2 Visualization of Personalized Chinese Adult Mesh-type Phantoms

Fig. 3 Visualization of the personalized Chinese adult mesh-type phantom library with skin and soft tissue removed. From left to right: underweight, normal-weight, overweight, and obese body sizes.

Table 4 Organ masses (g) of the Chinese adult male phantom and their relative differences with respect to the reference data in GBZ/T 200.2–2007 "Masses of main organs and tissues" .

Organs	CAMP-M	MRCP-AM[19]	GBZ/T	Relative error (%) (MRCP)	Relative error (%) (CAMP)
Thyroid	-	-	-	16.75%	4.75%
Heart	-	-	-	4.10%	1.04%
Liver	-	-	-	67.38%	2.44%
Gallbladder	-	-	-	15.11%	10.11%
Kidneys	-	-	-	27.16%	6.06%
Spleen	-	-	-	47.35%	3.89%
Stomach	-	-	-	27.79%	1.85%
Pancreas	-	-	-	44.69%	8.08%
Bladder	-	-	-	19.30%	7.53%
Testes	-	-	-	6.90%	6.93%
Oesophagus	-	-	-	24.45%	0.80%
Brain	-	-	-	3.93%	1.55%
Adrenals	-	-	-	24.00%	5.64%
Colon	-	-	-	7.44%	2.16%
Small intestine	-	-	-	39.05%	3.89%
Prostate	-	-	-	-	-
Breasts	-	-	-	-	-

Table 5 Organ masses (g) of the Chinese adult female phantom and their relative differences with respect to the reference data in GBZ/T 200.2–2007 "Masses of main organs and tissues" .

Organs	CAMP-F	MRCP-AF[19]	GBZ/T	Relative error (%) (MRCP)	Relative error (%) (CAMP)
Thyroid	-	-	-	14.44%	7.59%
Heart	-	-	-	1.07%	11.81%
Liver	-	-	-	40.31%	9.53%
Gallbladder	-	-	-	17.16%	4.29%
Kidneys	-	-	-	5.48%	4.84%
Spleen	-	-	-	24.93%	2.80%

Organs	CAMP-F	MRCP-AF[19]	GBZ/T	Relative error (%) (MRCP)	Relative error (%) (CAMP)
Stomach	-	-	-	50.01%	10.35%
Pancreas	-	-	-	44.55%	2.72%
Bladder	-	-	-	31.53%	4.13%
Ovaries	-	-	-	14.87%	1.82%
Oesophagus	-	-	-	37.49%	8.03%
Brain	-	-	-	1.47%	0.99%
Adrenals	-	-	-	18.97%	3.69%
Colon	-	-	-	74.25%	9.35%
Small intestine	-	-	-	67.96%	12.61%
Uterus	-	-	-	-	-
Breasts	-	-	-	70.77%	12.51%

Table 6 Organ masses (g) of selected organs in Chinese adults with four different body sizes.

Organs	Underweight Female	Normal Weight Female	Overweight Female	Obese Female
Brain	1447.65	1458.75	1469.11	1480.95
Heart	295.66	348.61	398.03	454.51
Kidneys	111.81	120.81	129.21	138.81
Liver	1174.19	1264.19	1348.19	1444.19
Pancreas	86.82	109.22	126.82	151.62
Spleen	151.64	153.04	154.14	155.69
	(1305.64)	(1329.86)	(1348.89)	(1375.70)
	(274.27)	(305.62)	(334.88)	(368.32)
	(150.72)	(159.87)	(168.41)	(178.17)
	(241.24)	(261.68)	(277.74)	(300.37)
	(250.94)	(283.98)	(309.94)	(346.52)

(*) indicates reference values calculated from the equation of Table 1.

Table 7 Human dimensions (cm) of Chinese adults with four different body sizes.

Human Dimensions	Underweight Female	Normal Weight Female	Overweight Female	Obese Female
Upper arm circumference	-	-	-	-
Chest circumference	-	-	-	-
Waist circumference	-	-	-	-
Hip circumference	-	-	-	-
Thigh circumference	-	-	-	-

3.2 Results of CT Dose Simulations

During ATCM scans, the tube current varies across different axial slices, resulting in varying CTDI(*{vol}) values for each slice. Correlation analysis is then performed to derive the relationship between organ doses and CTDI(*{vol}), DLP, and SSDE. Representative fitted curves and conversion coefficients for selected organs are shown in Fig. 4 [FIGURE:4]. The correlations between CTDI(*{vol}) and the doses of the lungs, heart, liver, kidneys, pancreas, and spleen are 0.96, 0.96, 0.95, 0.87, 0.87, and 0.84, respectively. Correlation analysis is performed to establish the relationship between organ doses and the mean DLP (DLP(*{mean})). The correlations between DLP(*{mean}) and the doses of the lungs, heart, liver, kidneys, pancreas, and spleen were 0.87, 0.88, 0.89, 0.80, 0.71, and 0.87, respectively. Correlation analysis is performed to establish the relationship between organ doses and the mean SSDE (SSDE(*{mean})). The correlations between SSDE(*{mean}) and the doses of the lungs, heart, liver, kidneys, pancreas, and spleen were 0.98, 0.99, 0.98, 0.95, 0.94, and 0.87, respectively. SSDE exhibits a stronger correlation with organ doses compared to CTDI(*{vol}) and DLP based on these results. We further demonstrate that patient-specific dose metrics, which account for individual body habitus, provide a more accurate assessment of organ dose levels.

Our study further demonstrates that patient-specific dose indices that account for individual body characteristics can more accurately assess organ dose levels, consistent with the findings of Franck et al. [**?**]. This linear relationship facilitates rapid clinical estimation of organ doses in CT examinations. Future research will build upon the individualized Chinese adult mesh-type phantom population developed in this study to further investigate personalized optimization strategies for low-dose CT scanning. By incorporating variations in radiation absorption and dose distribution among individuals with different body sizes, scanning parameters can be precisely adjusted to minimize patient radiation exposure while maintaining image quality. In addition, Monte Carlo–based

dose assessment results will be employed to validate the effectiveness and safety of the individualized scanning protocols. This work not only contributes to the establishment of low-dose CT optimization strategies tailored to the Chinese population but also provides a solid theoretical and technical foundation for the development of personalized imaging protocols in clinical practice, thereby enhancing both the safety and precision of CT examinations.

Fig. 4 Relationship between organ doses and CTDI(_{vol}), DLP and SSDE for selected organs.

4. Conclusion

In this study, a library of mesh-type phantoms reflecting the personalized characteristics of Chinese adults is established, providing a solid foundation for CT radiation dose assessment and supporting further clinical research related to CT dose. The methodology includes medical image acquisition, organ modeling and optimization, and model assembly, ultimately resulting in a cohort of individualized phantoms representative of Chinese adults. Furthermore, we examine the relationships between organ mass and body weight, as well as between anthropometric dimensions and height and weight, and establish quantitative linear regression equations to serve as reference values for constructing individualized phantoms. The results indicate that the organ masses and body dimensions of the CAMP series mesh-type phantoms developed in this study better represent the anatomical characteristics of Chinese adults, making them more suitable for evaluating and optimizing CT radiation doses in Chinese patients. In addition, we investigate the relationships between organ doses and the clinical dose indices CTDI(_{vol}), DLP, and SSDE. The experimental results show that SSDE exhibited a stronger correlation with organ doses. Overall, the individualized Chinese adult mesh phantom library developed in this study provides an essential tool for subsequent CT radiation dose assessments.

Acknowledgments: This work was supported by the National Natural Science Foundation of China (No. 82271988, U1867210 and 62227804), Beijing Scholar 2015 (Zhenchang Wang), and Beijing Hospitals Authority Clinical Medicine Development of code: YGLX202501.

References

1. Y. Niu, Y. Zhang, W. Zhuo, et al., The necessity and countermeasure of strengthening radiation dose management in diagnostic radiology, Chin. J. Radiol. Med. Prot. 43, 241-247 (2023). https://doi.org/10.3760/cma.j.cn112271-20221205-00469
2. Y. Niu, Y. Su, J. Liang, et al., Study on estimation of medical exposure frequency in China, Chin. J. Radiol. Med. Prot. (2019). https://doi.org/10.3760/cma.j.issn.0254-5098.2019.05.002
3. United Nations Scientific Committee on the Effects of Atomic Radiation, UNSCEAR 2020/2021 report. Evaluation of medical exposures to ionizing radiation, New York: UNSCEAR (2022)

4. M. M. Rehani, K. Yang, E. R. Melick, et al., Patients undergoing recurrent CT scans: assessing the magnitude, Eur. Radiol. 30, 1828–1836 (2020). https://doi.org/10.1007/s00330-019-06523-y
5. R. Smith-Bindman, P. W. Chu, H. Azman Firdaus, et al., Projected Lifetime Cancer Risks From Current Computed Tomography Imaging, JAMA Intern. Med. 185, 710–719 (2025). https://doi.org/10.1001/jamainternmed.2025.0505
6. M. Bosch de Basea Gomez, I. Thierry-Chef, R. Harbron, et al., Risk of hematological malignancies from CT radiation exposure in children, adolescents and young adults, Nat. Med. 29, 3111–3119 (2023). https://doi.org/10.1038/s41591-023-02620-0
7. H. Schlattl, M. Zankl, J. Becker, et al., Dose conversion coefficients for CT examinations of adults with automatic tube current modulation, Phys. Med. Biol. 55, 6243 (2010). https://doi.org/10.1088/0031-9155/55/20/013
8. E. Samei, F. Ria, X. Tian, et al., A database of 40 patient-based computational models for organ dose estimates benchmarking in CT, Med. Phys. (2020). https://doi.org/10.1002/mp.14373
9. P. Zhao, G. Ning, W. Bingzhi, et al., A Review of Computational Phantoms for Quality Assurance in Radiology and Radiotherapy in the Deep-Learning Era, 방사선방어학회지 47, 111–133 (2022). https://doi.org/10.14407/jrpr.2021.00402
10. M. Zankl, G. Drexler, N. Petoussi-Henss, et al., The calculation of dose from external photon exposures using reference human phantoms and Monte Carlo methods. Pt. 7. Organ doses due to parallel and environmental exposure geometries (1997)
11. W. S. Snyder, M. R. Ford, G. G. Warner, et al., Estimates of absorbed fractions for monoenergetic photon sources uniformly distributed in various organs of a heterogeneous phantom., J Nucl Med 10 Suppl No 3 7-52 Aug 1969 (1969)
12. X. G. Xu, T. C. Chao, and A. Bozkurt, VIP-MAN: An Image-Based Whole-Body Adult Male Model Constructed From Color Photographs Of The Visible Human Project For Multi-Particle Monte Carlo Calculations, Health Phys. 78, 476 (2000)
13. A. M. Geyer, S. O'Reilly, C. Lee, et al., The UF/NCI family of hybrid computational phantoms representing the current US population of male and female children, adolescents, and adults—application to dosimetry, Phys. Med. Biol. (2014). https://doi.org/10.1088/0031-9155/59/18/5225
14. N. Petoussi-Henss, M. Zanki, U. Fill, et al., The GSF family of voxel phantoms, Phys. Med. Biol. 47, 89–106 (2002). https://doi.org/10.1088/0031-9155/47/1/307
15. X. G. Xu, An exponential growth of computational phantom research in radiation protection, imaging, and radiotherapy: a review of the fifty-year history, Phys. Med. Biol. 59, R233-302 (2014). https://doi.org/10.1088/0031-9155/59/18/R233
16. W. Kainz, E. Neufeld, W. E. Bolch, et al., Advances in Computational Human Phantoms and Their Applications in Biomedical Engineering—A

Topical Review, IEEE Trans. Radiat. Plasma Med. Sci. 3, 1–23 (2019). https://doi.org/10.1109/TRPMS.2018.2883437
17. W. Segars, B. Tsui, D. Lalush, et al., Development and application of the new dynamic Nurbs-based Cardiac-Torso (NCAT) phantom., J. Nucl. Med. (2001)
18. J. Zhang, Y. H. Na, P. F. Caracappa, et al., RPI-AM and RPI-AF, a pair of mesh-based, size-adjustable adult male and female computational phantoms using ICRP-89 parameters and their calculations for organ doses from monoenergetic photon beams, Phys. Med. Biol. 54, 5885 (2009). https://doi.org/10.1088/0031-9155/54/19/015
19. International Commission on Radiological Protection, ICRP Publication 145 Adult mesh-type reference computational phantoms, Ann. ICRP 49(3) (2020)
20. S. Kim, B. Shin, C. Choi, et al., Pediatric phantom library constructed from ICRP mesh-type reference phantoms (MRCPs), Nucl. Technol. (2024). https://doi.org/10.1016/j.net.2024.03.022
21. S. Kim, B. Shin, H. Kim, et al., Body-size-dependent pediatric phantom library constructed from ICPR pediatric mesh-type reference computational phantoms, KNS 2022 Fall Conf. 2022 추계학술발표회, 1–3 (2022)
22. R. Ma, R. Qiu, Z. Wu, et al., Development of Chinese mesh-type pediatric reference phantom series and application in dose assessment of Chinese undergoing computed tomography scanning, Phys. Med. Biol. 66, 195002 (2021). https://doi.org/10.1088/1361-6560/ac1ef1
23. X. Luo, R. Qiu, Z. Wu, et al., A body-size-dependent series of Chinese adult standing phantoms for radiation dosimetry, Radiol. Prot. (2023). https://doi.org/10.1088/1361-6498/acad0d
24. T. Xie, A. Akhavanallaf, and H. Zaidi, Construction of patient-specific computational models for organ dose estimation in radiological imaging, Med. Phys. 46, 2403–2411 (2019). https://doi.org/10.1002/mp.13471
25. S. Huang, Q. Liu, and T. Xie, Chinese reference population: Open-source age-dependent computational phantoms of reference Chinese population, Med. Phys. 52, 2688–2696 (2025). https://doi.org/10.1002/mp.17670
26. T. Xie, P.-A. Poletti, A. Platon, et al., Assessment of CT dose to the fetus and pregnant female patient using patient-specific computational models, Eur. Radiol. 28, 1054–1065 (2018). https://doi.org/10.1007/s00330-017-5000-z
27. G. L. de la Grandmaison, I. Clairand, and M. Durigon, Organ weight in 684 adult autopsies: new tables for a Caucasoid population, Forensic Sci. Int. 119, 149–154 (2001). https://doi.org/10.1016/S0379-0738(00)00401-1
28. M. D. Bell, T. Long, A. C. Roden, et al., Updating Normal Organ Weights Using a Large Sample Database, Arch. Pathol. Lab. Med. (2022). https://doi.org/10.5858/arpa.2021-0287-OA
29. J. Wang and R. Chen, Data of Anatomical Physiological and Metabolic Characteristics for Chinese Reference Man (1998)
30. Standardization Administration of the People's Republic of China, Human dimensions of Chinese adults, GB/T 10000-2023 (2023)

31. J. Wasserthal, H.-C. Breit, M. T. Meyer, et al., TotalSegmentator: robust segmentation of 104 anatomical structures in CT images, Radiol. Artif. Intell. (2023). https://doi.org/10.1148/ryai.230024
32. T. A. D' Antonoli, L. K. Berger, A. K. Indrakanti, et al., TotalSegmentator MRI: Robust Sequence-independent Segmentation of Multiple Anatomic Structures in MRI, Radiology 314, e241613 (2025). https://doi.org/10.1148/radiol.241613
33. H. Han, Y. S. Yeom, C. Choi, et al., POLY2TET: a computer program for conversion of computational human phantoms from polygonal mesh to tetrahedral mesh, J. Radiol. Prot. 40, 962–979 (2020). https://doi.org/10.1088/1361-6498/abb360
34. C. Ge, Research on Deformation Technology and Application of Chinese Radiation Protection Reference Man (2014)
35. S. Agostinelli, J. Allison, K. Amako, et al., Geant4—a simulation toolkit, Nucl. Instrum. Methods Phys. Res. Sect. Accel. Spectrometers Detect. Assoc. Equip. 506, 250–303 (2003). https://doi.org/10.1016/S0168-9002(03)01368-8
36. J. Allison, K. Amako, J. Apostolakis, et al., Geant4 developments and applications, IEEE Trans. Nucl. Sci. 53, 270–278 (2006). https://doi.org/10.1109/TNS.2006.869826
37. D. Sarrut, M. Bała, M. Bardiès, et al., Advanced Monte Carlo simulations of emission tomography imaging systems with GATE, Phys. Med. Biol. 66, 10TR03 (2021). https://doi.org/10.1088/1361-6560/abf276
38. J. Punnoose, J. Xu, A. Sisniega, et al., Technical Note: spektr 3.0—A computational tool for x-ray spectrum modeling and analysis, Med. Phys. (2016). https://doi.org/10.1118/1.4955438
39. K. Yang, X. Li, X. George Xu, et al., Direct and fast measurement of CT beam filter profiles and simultaneous geometrical calibration, Med. Phys. (2017). https://doi.org/10.1002/mp.12024
40. X. Li, J. Q. Shi, D. Zhang, et al., A new technique to characterize CT scanner bow-tie filter attenuation and applications in human cadaver dosimetry simulations, Med. Phys. 42, 6274–6282 (2015). https://doi.org/10.1118/1.4932364
41. W. Zhao, K. Niu, S. Schafer, et al., An indirect transmission measurement-based spectrum estimation method for computed tomography, Phys. Med. Biol. 60, 339–357 (2015). https://doi.org/10.1088/0031-9155/60/1/339
42. K. Yang, C. Ruan, X. Li, et al., Data of CT bow tie filter profiles from three modern CT scanners, Data Brief 25, 104261 (2019). https://doi.org/10.1016/j.dib.2019.104261
43. A. Akhavanallaf, T. Xie, and H. Zaidi, Assessment of uncertainties associated with Monte Carlo-based personalized dosimetry in clinical CT examinations, Phys. Med. Biol. 65, 045008 (2020). https://doi.org/10.1088/1361-6560/ab6b45
44. C. Franck, C. Vandevoorde, I. Goethals, et al., The role of Size-Specific Dose Estimate (SSDE) in patient-specific organ dose and cancer risk estimation in paediatric chest and abdominopelvic CT examinations, Eur.

Radiol. 26, 2646–2655 (2016). https://doi.org/10.1007/s00330-015-4091-7